ACS OMEGA

http://pubs.acs.org/journal/acsodf

Article

High-Thermal-Conductivity and High-Fluidity Heat Transfer Emulsion with 89 wt % Suspended Liquid Metal Microdroplets

Suyeon Kim, Seongeun Kang, and Joohyung Lee*

Cite This: *ACS Omega* 2023, 8, 17748−17757

Read Online

ACCESS | Metrics & More | Article Recommendations | Supporting Information

ABSTRACT: Colloidal suspensions of thermally conductive particles in a carrier fluid are considered promising heat transfer fluids for various thermal energy transfer applications, such as transportation, plants, electronics, and renewable energy systems. The thermal conductivity (k) of the particle-suspended fluids can be improved substantially by increasing the concentration of conductive particles above a "thermal percolation threshold," which is limited because of the vitrification of the resulting fluid at the high particle loadings. In this study, eutectic Ga−In liquid metal (LM) was employed as a soft high-k filler dispersed as microdroplets at high loadings in paraffin oil (as a carrier fluid) to produce an emulsion-type heat transfer fluid with the combined advantages of high thermal conductivity and high fluidity. Two types of the LM-in-oil emulsions, which were produced via the probe-sonication and rotor−stator homogenization (RSH) methods, demonstrated significant improvements in k, i.e., Δk ∼409 and ∼261%, respectively, at the maximum investigated LM loading of 50 vol % (∼89 wt %), attributed to the enhanced heat transport via high-k LM fillers above the percolation threshold. Despite the high filler loading, the RSH-produced emulsion retained remarkably high fluidity, with a relatively low viscosity increase and no yield stress, demonstrating its potential as a circulatable heat transfer fluid.

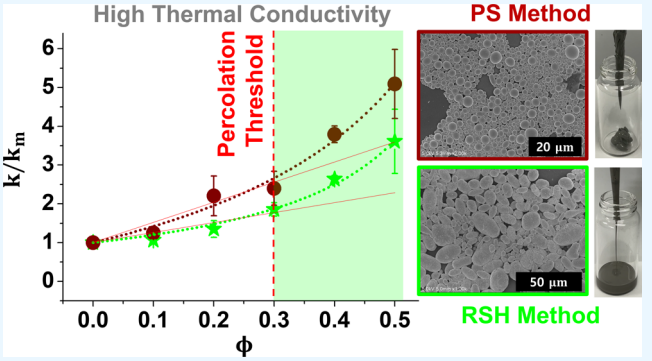

1. INTRODUCTION

Fluids are widely utilized as heat carriers in daily life and in various industrial areas where thermal energy transfer and utilization are required, including buildings,[1,2] transportation,[3,4] manufacturing plants,[5] electronics,[6−8] and solar thermal systems.[9,10] The thermal conductivity (k) of a heat transfer fluid is an important parameter in the applications. Significant efforts have been made to improve the k of commonly used heat transfer fluids (e.g., water, ethylene glycol, and paraffinic or silicone oils), which are pure liquids with relatively low k values, by adding highly conductive solid particles (e.g., metal,[11−13] ceramic,[14−16] or carbon-based[17−19]). The resulting fluids in the form of a colloidal suspension, often termed "nanofluids"[20−23] because of the sizes of the dispersed particles typically in the nanometer range, exhibit higher k values than those of the base fluids. Nanofluids with improved k values have shown promising performances in applications such as solar thermal collectors,[24,25] electronic cooling,[26] and heat exchangers.[27,28] The k value of the heat transfer fluid depends not only on the type of the dispersed particles but also on their concentration.[29] Typically explored particle concentrations for nanofluids range from ∼0.01 to a few percent (e.g., ∼5%),[21−23] where the increases in k, as compared to those of the base fluids, range from a few to a few tens of % (e.g., ∼50%).[11−23] At higher particle concentrations, the viscosity of the resulting colloidal suspension can significantly increase,[22,23] possibly accompanying particle aggregation and thus causing clogging, which limits its practical applicability in the most relevant geometries. Although not many, some exceptionally high enhancements of the k values with the addition of conductive particles have also been reported. For instance, Choi et al.[30] reported an anomalously high k-value enhancement of ∼150% with respect to that of the base fluid for the nanofluids containing multiwalled carbon nanotubes at a relatively low particle concentration of 1 vol %. However, this is accompanied by a steep increase in viscosity by approximately three orders of magnitude,[22] which is undesirable in practical applications of the resulting fluid, where its prolonged circulation is crucial. Evidently, the addition of conductive particles in a liquid medium results in a trade-off between thermal conductivity and viscosity. This could be the reason why a majority of nanofluid research studies have paid relatively little attention to potential systems with even higher particle concentrations than typically explored regions.

Received: January 24, 2023
Accepted: April 25, 2023
Published: May 9, 2023

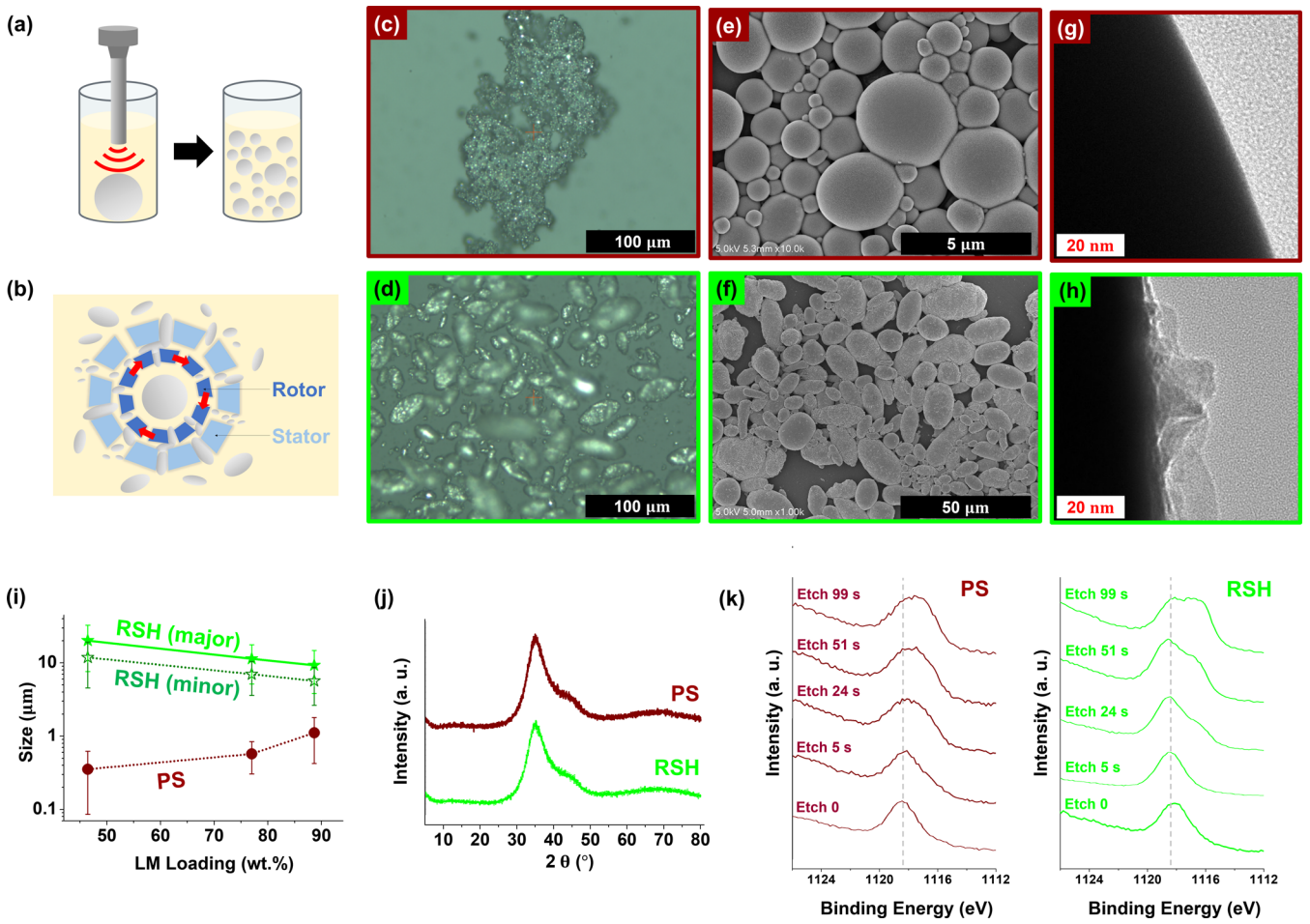

Figure 1. Schematic illustrations of the two emulsification methods used in this study: (a) probe-sonication (PS) and (b) rotor−stator homogenization (RSH). Optical micrographs of the (c) PS- and (d) RSH-produced emulsions. Scanning electron microscopy (SEM) images of (e) PS- and (f) RSH-produced LM droplets. Transmission electron micrographs of the edges of the (g) PS- and (h) RSH-produced LM droplets. (i) Sizes of the LM droplets produced at various LM loadings (10, 30, and 50%) using the two emulsification methods (circles: PS, stars: RSH; the solid and hollow marks for the RSH indicate the major and minor diameters, respectively, of the anisotropic LM droplets produced in this method), inferred from the SEM images (Figure S1 in the Supporting Information). (j) X-ray diffraction patterns (upper: PS, lower: RSH) and (k) narrow-scan X-ray photoelectron spectroscopy analysis of the LM droplets produced by the two emulsification methods (left: PS, right: RSH). The dashed vertical line indicates the characteristic peak corresponding to the gallium oxide observed at the outermost surface of the LM droplets.

Without considering the upper particle concentration limit constrained by the loss of fluidity of the nanofluid, it is theoretically[31−34] anticipated that a higher concentration of high-k particles in a (low-k) matrix would yield a higher overall k value of the mixture. This has been demonstrated in different contexts for numerous free-standing polymer composites[35−39] consisting of solid particles (termed "fillers;" dispersed phase) and a solidified polymer matrix (continuous phase), with high and low k values, respectively. Although the k value of the matrix (e.g., ∼0.2 W/(m·K) for epoxy)[37] is often as low as those of the base fluids for nanofluids (e.g., ∼0.2 W/(m·K) for mineral oils), the overall k values reported for the polymer composites containing high-k fillers (of similar materials as the particles for nanofluids) are very high, e.g., ∼11 W/(m·K) for a graphene-filled epoxy composite at a 45 vol % filler loading, corresponding to a ∼5400% enhancement in the k value with respect to that of the matrix.[37] Similarly, in most reported cases,[35] the enhancements in the k values for polymer/filler composites significantly exceeded those for nanofluids. Notably, the typical filler concentrations of polymer/filler composites with high overall k values are above the "percolation threshold,"[31,32,40] where the thermal transport through the dispersed phase (i.e., the network of fillers) becomes effective, which often far exceeds the particle concentration ranges studied for nanofluids. Because most thermal management applications where free-standing polymer composites are mainly utilized (e.g., packaging)[41] do not require a high sample fluidity, increasing the particle concentration up to such high levels generally does not cause any considerable problem.

Recently, liquid metals (LMs), particularly Ga and Ga-based alloys, have received considerable attention in the development of high-k composites for thermal management applications,[42−47] based on their integrated advantages of high conductivity, high fluidity, and low toxicity.[48] In the manufacturing of polymer-based composites, LMs can be easily dispersed as micro- or nanosized entities using various physical methods such as shear mixing[42,44−46] or sonication,[47] and "emulsified" into a continuous prepolymer liquid that can be subsequently cured to form a polymeric matrix. Besides the high k values (e.g., ∼26.4 W/m·K for eutectic Ga−In or EGaIn),[49] the high deformability of such metals, as being in

https://doi.org/10.1021/acsomega.3c00487
ACS Omega 2023, 8, 17748−17757

the liquid state at room temperature, is considered a unique and important property in the fabrication of stretchable elastomers, and potentially future form-factor-free composite materials.[45] Furthermore, the deformability of LMs may allow for higher loadings in the matrix than the maximum packing density of conventional rigid solid fillers.[46]

To date, as thermally conductive fillers, LMs have been utilized exclusively in solidifiable matrices; however, their functionality in a purely liquid matrix has rarely gained attention. In this study, we considered a colloidal system of LM droplets dispersed in a nonsolidifiable liquid medium as a new type of heat transfer fluid with high k and high fluidity. Specifically, EGaIn, which is a focused LM with a melting point below room temperature,[48] was dispersed in liquid paraffin,[23] which is a widely used base fluid for conventional nanofluids. Two different processes were employed in LM dispersion: (1) the previously known and widely used probe-sonication (PS) method[50−52] and (2) the rotor−stator homogenization (RSH) method, which has been used to manufacture various emulsion systems of conventional immiscible liquids (e.g., oil-in-water (o/w) or water-in-oil (w/o))[53,54] but not frequently for LMs. The RSH method, based on high shear force, produces anisotropic LM droplets with large dimensions (≥10 μm in major diameter and ≥5 μm in minor diameter), in contrast to the isotropic submicron LM droplets produced via the PS method. Although both types of colloidal systems exhibited a remarkable increase in k up to several hundred % with respect to the base fluid with increasing LM loadings above percolation thresholds, the RSH-based system with larger anisotropic LM droplets showed higher "fluidity," even at an extremely high filler weight loading of 89 wt %, demonstrating its high potential as a circulatable heat transfer fluid.

2. RESULTS AND DISCUSSION

Figure 1a,b shows the schematic illustrations of the two LM (EGaIn) dispersion methods investigated in this study. Paraffin oil was selected as the carrier fluid (or the continuous phase of the emulsion, where EGaIn was the dispersed phase) owing to its chemical inertness and thermal stability (boiling point of 300 °C), which are suitable for various practical heat exchange applications.[22,23] The carrier fluid was preliminarily doped with an oil-soluble surfactant, aerosol OT (AOT, 150 mM), which induces electrostatic surface charging and thereby improves the colloidal stability of LM droplets dispersed in nonpolar media.[51]

Figure 1c,e shows the representative optical microscopy (OM) and scanning electron microscopy (SEM) images of the LM droplets, respectively, obtained via PS at an LM loading of 50 vol % (∼89 wt %). Individual droplets were not discernible via OM (Figure 1c) because of their small sizes, whereas SEM revealed that the droplets produced via the strong acoustic energy[55,56] applied in this method were spherical with an approximate average diameter of 1.1 ± 0.7 μm, which is consistent with the literature.[52] The spherical shape of the produced LM droplets is attributed to the high interfacial tension.[48,51] The droplets did not undergo coalescence and remained as discrete particles even after removing the carrier fluid, owing to the generation of a thin solid oxide skin,[48] as observed in the transmission electron microscopy (TEM) image of the outermost surface of an LM droplet (Figure 1g).

Figure 1d,f shows the OM and SEM images of the LM droplets produced via RSH at the same LM loading (50 vol %). The sample manufacturing tool used here is a typical benchtop homogenizer widely used for the preparation of conventional liquid-in-liquid (e.g., o/w[54] or w/o[53]) emulsions, which has not yet been frequently used for the preparation of LM emulsions. The shear force applied to the sample in this method is typically considered significantly lower than the physical force involved in the sonication method.[56,57] Thus, the sizes of the LM droplets produced were significantly larger than those produced via the PS method, such that the individual droplets were discernible in the OM (Figure 1d). Furthermore, in stark contrast to the spherical droplets produced in the PS method, the shapes of the LM droplets produced in the RSH method exhibited a significant anisotropy with 9.3 ± 5.5 μm in major and 5.7 ± 3.0 μm in minor diameters estimated for a sample emulsion prepared at an LM loading of 50 vol % (Figure 1f). Similar "micro-rice" droplets have been produced on a small scale using a microfluidic device,[58] and "nano-rice" droplets,[59] with submicron sizes, have also been reported, which were produced via sonication in aqueous media. The latter method, i.e., sonication in aqueous media, accompanied the generation of gallium oxyhydroxide (GaOOH) crystalline phase as a consequence of the chemical reaction between Ga and water,[60] which often resulted in the formation of "nanorods" with higher aspect ratios.[59,60] However, no strong evidence for the formation of the GaOOH phase was observed in the X-ray diffraction (XRD) pattern (Figure 1j) of the anisotropic LM droplets produced from RSH in the nonpolar surfactant solution used in this study. The XRD patterns for the LM droplets produced from the two methods used in this study were practically the same, which revealed the amorphous nature of the products, suggesting that both products retained the properties of the bulk liquid. Thus, the formation of anisotropic rice-like LM droplets shown here cannot be attributed to the formation of a new crystalline phase such as GaOOH. A likely mechanism is that the LM droplets passing through the narrow channels between the rotor and stator were subject to a strong shear force and mechanically deformed in the direction of shear,[58] and subsequently, the deformed droplets retained their anisotropic shapes owing to the solid oxide (likely gallium oxide, Ga_2O_3)[48,51] skin formed at the outermost surface. Notably, previous studies in which mechanical shear force was similarly utilized to form LM droplets, but without confining them to a narrow channel, mostly reported spherical droplet shapes,[61,62] which is qualitatively different from the micro-rice-like droplets produced via the RSH method.

Figure 1i illustrates the variations in the average sizes of the LM droplets produced by the two methods with different LM loadings (the SEM images for the respective samples are shown in the Supporting Information, Figure S1). In the PS method, the sizes of the produced LM droplets gradually increased (e.g., from ∼300 nm at ∼46 wt % to ∼1 μm at ∼89 wt %), indicating that the emulsification efficiency slightly decreased with the increasing LM loading. In the RSH method, the sizes of the LM droplets decreased with increasing LM loading, which is because larger amounts of LM droplets passing through channels with fixed widths were subject to stronger shear forces, leading to a higher milling effect. The surface of the LM droplets produced via RSH was not smooth (Figure 1f,h), mimicking the wrinkled oxide structure observed on a macroscopic LM droplet under mechanical compression.[63] This structure was probably generated during the course of shear milling, which continually caused mechanical deformation of the circulating LM droplets, consistent with the

https://doi.org/10.1021/acsomega.3c00487
ACS Omega 2023, 8, 17748−17757

proposed mechanisms for droplet shape anisotropy. For a detailed understanding of the surface compositions, depth profile analysis was conducted by performing X-ray photoelectron spectroscopy (XPS) with Ar ion beam etching. In the resulting narrow-scan spectra for the RSH-produced sample (Figure 1k, right), the characteristic Ga $2p_{3/2}$ peak at ∼1118 eV, corresponding to Ga(III) (i.e., Ga_2O_3), was discerned for a prolonged etching time (up to 99 s). However, for the PS-produced sample (Figure 1k, left), the peak shifted to that at a lower binding energy, corresponding to Ga(0) (i.e., metallic Ga) at a shorter etching time. This suggests that thicker oxide layers were formed on the surface of the RSH-produced LM droplets, which is consistent with the TEM observations (Figure 1h).

Figure 2a illustrates the thermal conductivity values measured for the LM-in-oil emulsions with different LM loadings prepared using the two methods. The overall k value of the emulsion (to be denoted without a subscript) increased remarkably as the loading of LM with a high k value (k_f = 26.4 W/m·K,[49] where the subscript f indicates the "filler") increased. Notably, the increases in the emulsion k values, i.e., Δk (%) = $(k - k_m)/k_m \times 100$ (k_m = 0.193 W/m·K, where the subscript m indicates the "matrix," that is, the surfactant solution), at the maximum investigated LM loading (50 vol %), were 409 and 261% for the emulsions generated via the PS and RSH methods, respectively. These values were higher by orders of magnitudes than the typically reported values (i.e., Δk (%) only of a few to a few tens of %) for various nanofluids demonstrated in the literature,[21−23] with maximum conductive filler loadings only of a few vol % or lower. Furthermore, the measured Δk (%) values for both LM-in-oil emulsions at 50 vol % LM loading were comparable to those of some free-standing solid polymer composites containing thermally conductive fillers at similar loadings (e.g., Δk (%) ∼250% for graphite fibers in epoxy resin[32]). Interestingly, a recently reported "reverse" colloid, wherein silicone oil is dispersed in the LM matrix (i.e., oil-in-LM emulsion),[64] has a much higher k value than the LM-in-oil colloids of this study, probably because of the high electrical conductivity of the metallic continuous phase. Meanwhile, the LM-in-oil colloids, wherein LM is dispersed in an insulating oil matrix, are electrically insulating and thus are of practical relevance to thermal transport applications where electrical insulation is crucial. Furthermore, in stark contrast to the oil-in-LM system, the current LM-in-oil system, particularly that produced via the RSH method, exhibits high flowability, which is important for a circulatable heat transfer fluid (to be discussed later). We observed no significant increase in the k value from that of the pristine paraffin oil with an increase in the amount of added surfactants up to 150 mM (the concentration of the matrix surfactant solution; Figure S2 in the Supporting Information); therefore, the increase in the k values is mostly attributed to the increase in the loading of LM droplets as thermally conductive fillers dispersed in the carrier fluid. Importantly, neither system was completely vitrified, even at the maximum LM loading (50 vol %), retaining the fluid-like properties (although there was a clear difference in the fluidity between the two systems, to be discussed later), in contrast to the conventional colloidal suspensions containing solid particles at the corresponding particle loading.[65,66]

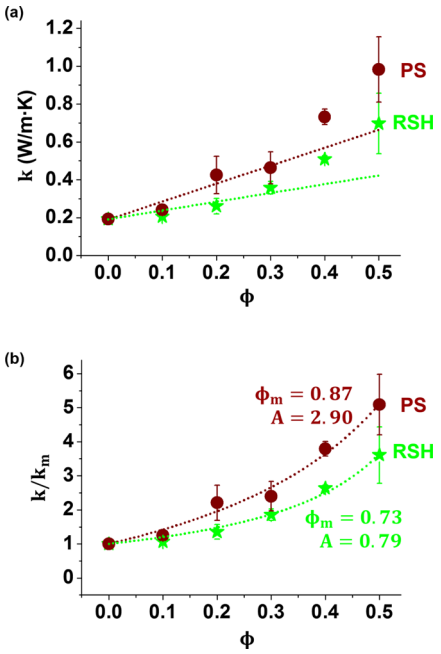

Figure 2. (a) Thermal conductivity (k in W/m·K) of the PS- and RSH-produced LM-in-oil emulsions at various LM loadings (10−50 vol %); dotted straight lines represent the deviation from the linear relation between the k values and LM loadings. (b) Relative k values with respect to the matrix conductivity (k_m = 0.193 W/m·K), k/k_m; the data were fitted to the Lewis−Nielsen model (dotted curves); the fitted parameters are shown next to the respective fitting curves.

The onset of deviation from the linear relation between the k value and filler loading, that is, the transition from a linear to a super-linear relation, has been assumed to be the thermal percolation threshold[37,45] at which the heat can propagate via the network of fillers with a high k_f, in thermally conductive polymer composites. Such a transition was observed at LM loadings approximately between 20−30% for the liquid emulsion-type heat transfer fluids investigated here (Figure 2a; the dotted straight lines describe the initial proportionality between k/k_m and ϕ at low ϕ regions, i.e., $\phi \leq 0.3$). Note that the thermal percolation referred to herein is different from electrical percolation; the latter is unlikely to occur in the current LM-in-oil emulsions owing to the insulating oxide skin of the LM droplets and oil medium, as confirmed by a conductometer. Thus, the relative thermal conductivity values of the emulsions with various LM loadings to that of the LM-free carrier fluid, k/k_m (Figure 2b), were fitted with the classical Lewis−Nielsen model,[31,32] which considers the heat transport via the percolated filler network, and it is defined as

$$\frac{k}{k_m} = \frac{(1 + AB\phi)}{(1 - B\psi\phi)} \tag{1}$$

where

$$A = k_E - 1 \tag{2}$$

$$B = \frac{\left(\frac{k_f}{k_m} - 1\right)}{\left(\frac{k_f}{k_m} + A\right)} \tag{3}$$

$$\psi = 1 + \frac{(1 - \phi_m)}{(\phi_m^2)}\phi \tag{4}$$

https://doi.org/10.1021/acsomega.3c00487
ACS Omega 2023, 8, 17748−17757

and k_E is the generalized Einstein coefficient reflecting the characteristics of the fillers (e.g., shape and orientation with respect to the heat flow); ϕ and ϕ_m are the volume fraction and maximum packing fraction of the fillers in the matrix, respectively.

The fitting of the measured k/k_m values with eq 1, with no fixed values for the two variables, i.e., ϕ_m and A, resulted in the ϕ_m values of 0.87 and 0.73 for the emulsions from the PS and RSH methods, respectively (Figure 2b). A higher ϕ_m value for the PS product may be attributed to the smaller sizes and uniformly spherical shapes of the produced LM droplets, which could enable more efficient geometrical packing than the droplets from the RSH method having larger sizes and significant anisotropy.[67] Fitting parameter A describes the efficiency of heat transport, where $A \to \infty$ and $A \to 0$ correspond to the upper and lower bounds of the overall k value, respectively, for a mixture of high-k (k_f) and low-k (k_m) components.[32,45] As $A \to \infty$ (and $\phi_m = 1$), in which the eq 1 is reduced to the well-known "rule of mixtures ($k = (1 - \phi)k_m + \phi k_f$)," the heat transport occurs mainly through the percolated network of the high-k fillers, whereas as $A \to 0$, where eq 1 is reduced to the "inverse rule of mixtures ($1/k = (1 - \phi)/k_m + \phi/k_f$)," [68] the heat transport occurs mainly through the low-k matrix. The A values obtained for the emulsions from the PS and RSH methods were 2.90 and 0.79, respectively, which were within the ranges of some reported values for polymer/filler composites where the thermal transport was assumed to occur via the percolated filler network (e.g., A = 0.5 or 1 for graphite fibers in epoxy, A = 1.5 for glass spheres in polyethylene, and A = 3 for alumina in polystyrene).[32] A higher A value was obtained for the PS product, indicating that heat transport through the percolated network of fillers was more effective, which is consistent with the assumed higher packing efficiency in this system than in the RSH product.

One thing to be noted is that parameters ϕ_m and A obtained by fitting the experimental results with eq 1 are purely phenomenological,[69,70] given that the exact values of such parameters for LM droplets are not known. The obtained ϕ_m values of 0.87 and 0.73 for both systems are larger than a previously suggested value of ~0.64[71] for random close packing of monodisperse hard spheres, and furthermore, the ϕ_m of 0.87 for the sonication product is even larger than the theoretically maximum possible packing density of ~0.74. The large values obtained for the systems studied here may implicate the polydispersity[72,73] and even deformability[74] of the produced droplets, which are generally known to significantly affect the rheological properties of a colloid system. These values are practically difficult to predict theoretically; thus, they are empirical in nature, requiring due caution when interpreted quantitatively. Recently, Moon et al.[46] demonstrated that an extremely high loading of LM droplets in a polymer matrix, that is, up to 0.9, was possible owing to the deformability of LM droplets. Inspired by this study, the constrained fitting of the measured k/k_m values using eq 1 with a fixed of 1 was also performed, assuming that the deformability of LM droplets would enable the complete filling of dead volumes between the neighboring droplets that were not accessible by nondeformable solid particles (Figure S3). The obtained A values were 3.3 and 1.5 for the PS and RSH products, respectively, which are different from those obtained from the unconstrained fitting but still demonstrate a higher heat transport efficiency through the percolated LM droplets for the PS product.

A more efficient formation of the percolated network between the LM droplets in the PS product was beneficial for obtaining a higher k value, which could negatively affect the fluidity of the resulting emulsion, which is an important parameter for a circulatable heat transfer fluid. This conductivity−fluidity trade-off can be well appreciated by comparing the relative k values between the two types of LM-in-oil emulsions shown in Figure 2 with the rheological properties of the respective systems (Figures 3 and 4).

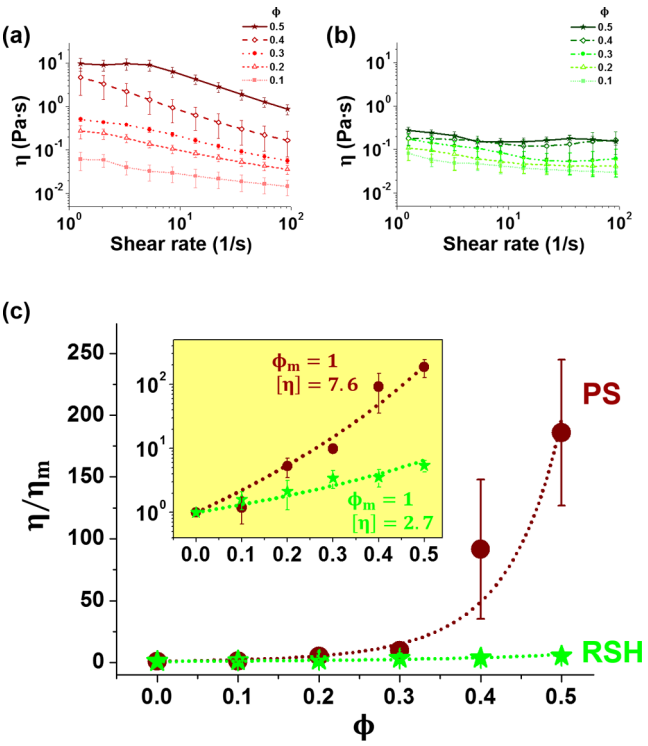

Figure 3. Viscosity (η in Pa·s) of the (a) PS- and (b) RSH-produced LM-in-oil emulsions at various LM loadings, measured in shear rate ranges between 10^0 and 10^2 s^{-1}. (c) Low-shear-rate η values (at 1.269 s^{-1}) divided by the matrix viscosity (η_m = 0.05 Pa·s), i.e., the relative viscosity η/η_m, plotted as functions of the LM loadings; the data were fitted to the Krieger−Dougherty model (dotted curves); the inset shows the equivalent data set in a log-scale y-axis, with the Krieger−Dougherty model fitting parameters.

Figure 3a,b illustrates the viscosities (η) of the PS and RSH products, respectively, with various LO loadings measured in a shear rate range of 1−100 s^{-1}. It is evident that the increase in η with increasing LM loading is significantly higher in the PS products. The increase in η in the PS products was remarkable at low-shear regions, and the samples with high LM loadings exhibited significant shear-thinning non-Newtonian behavior, which is in stark contrast to the case of the RSH products exhibiting significantly less shear and concentration dependences in all of the measured η values. The reduction in η for RSH products can be attributed to the significantly larger sizes of the suspended droplets (approximately an order of magnitude higher) compared with those of the PS products, resulting in a lower total particle surface area and higher particle deformability, both of which are known to decrease suspension viscosity.[67,74]

Figure 3c shows the η values of the emulsions at a low shear rate (1.269 s^{-1}) relative to the viscosity of the base fluid (η_m)

https://doi.org/10.1021/acsomega.3c00487
ACS Omega 2023, 8, 17748−17757

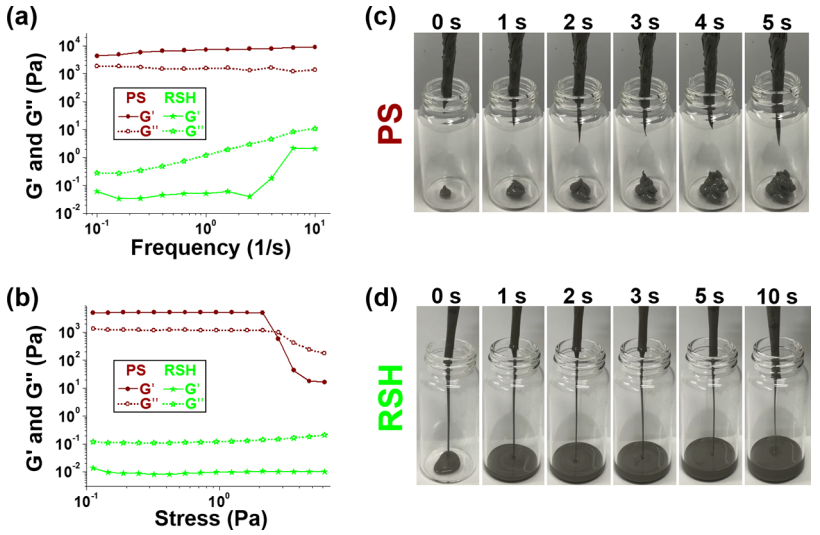

Figure 4. Elastic (G' in Pa, filled) and viscous (G'' in Pa, empty) moduli of the PS- (brown circles) and RSH-produced (green stars) LM-in-oil emulsions using (a) a frequency-sweep mode (0.1−10 s^{-1}) at a constant stress of 0.1 Pa and (b) a stress ramp (10^{-1}−10 Pa) at a constant frequency of 0.1 s^{-1} in oscillatory viscoelasticity measurements. Photographs contrasting the fluidity of the (c) PS- and (d) RSH-produced LM-in-oil emulsions at the maximum LM loading (50 vol %); the original video clips may be found in Supporting Movies S1 and S2.

as functions of the LM loading. Notably, the super-linear relation between η/η_m and LM loading (ϕ) is more significant than that between k/k_m and ϕ shown in Figure 2b, particularly for the PS product. The inset in Figure 3c shows the results of fitting the measured η/η_m values with the well-known Krieger−Dougherty equation,[75] which is given by

$$\frac{\eta}{\eta_m} = \left(1 - \frac{\phi}{\phi_m}\right)^{-[\eta]\phi_m} \quad (5)$$

where $[\eta]$ is the intrinsic viscosity that describes the contribution of the dispersed LM droplets to the overall sample η. The value of $[\eta]$ for a perfect sphere in a diluted suspension was suggested to be 2.5, which is consistent with the Einstein coefficient. Similar to our attempt to use the Lewis−Nielsen model to fit the measured k/k_m values, the Krieger−Dougherty equation is used to compare the sample thickening "efficiency" of the dispersed LM droplets in two different systems (i.e., PS vs RSH products) in a semi-quantitative fashion using the extracted empirical parameters. Interestingly, the fitting of the η/η_m values for various LM loadings with no fixed parameters resulted in $\phi_m = 1$, which was assumed above in the Lewis−Nielsen model fitting of k/k_m values. Furthermore, $[\eta] = 2.7$ for the RSH products was quite close to $k_E = A + 1 = 1.5 + 1 = 2.5$ extracted above for the same samples. This consistency between $[\eta]$ and k_E is remarkable, given that both parameters may be considered as the generalized Einstein coefficient, which is a measure of the contribution of a specific type of filler to the overall suspension property. In contrast, the extracted $[\eta]$ value for the sonication products, that is, $[\eta] = 7.6$, is significantly larger than $k_E = A + 1 = 3.3 + 1 = 4.3$ for the same samples. Considering the ratio of the k_E to $[\eta]$, which are related to the thermal percolation (a benefit; favored for a heat transfer fluid) and rheological percolation (a cost; disfavored), respectively, the resultant $k_E/[\eta]$ of ∼0.62 for the PS products indicates that these systems were less efficient in terms of translating the filler−filler interaction to the thermal transport than the RSH products with $k_E/[\eta] \sim 0.93$ (note: a crude but more straightforward comparison via the directly weighing Δk by $\Delta\eta$, where $\Delta\eta$ (%) = $(\eta - \eta_m)/\eta_m$ x 100 (η_m = 0.05 Pa·s) at the highest LM loading similarly revealed the inefficiency of the sonication product ($\Delta k/\Delta\eta \sim 0.02$) compared to the homogenization product ($\Delta k/\Delta\eta \sim 0.6$)). This inefficiency is attributed to the persistence of phonon scattering at the filler−filler and filler−matrix interfaces regardless of the degree of interfiller contact (at least within the investigated range of filler loading here).[76]

Figure 4a shows the elastic (G') and viscous (G'') moduli of the two types of emulsions (50 vol % LM loading), reflecting the solid- and liquid-like properties of the samples, respectively,[77] obtained in oscillatory viscoelasticity measurements using a frequency-sweep mode (0.1−10 s^{-1}) at a weak constant stress of 0.1 Pa. The measured G' for the PS product was dominant over the G'' values in the entire frequency range, which reveals the gel-like nature of the system, consistent with visual observation (Figure 4c and Supporting Information Movie S1). The oscillatory measurements using a stress ramp (10^{-1} to 10 Pa) at a constant frequency of 0.1 s^{-1} displays the linear viscoelastic region where $G' > G''$, and the "yield stress" (τ_y) of the sample, i.e., crossover point of the G' and G'' curves,[78] was estimated to be ∼2 Pa. The yield stress behavior may be undesirable for practical thermal transport applications, where continuous circulation of the fluid is required for a prolonged time, in terms of the pumping cost and possible clogging issue. In contrast, the RSH product exhibited a significantly higher fluidity at the same maximum LM loading (Figure 4d and Supporting Information Movie S2), with $G'' > G'$ for all of the investigated conditions in both the frequency-sweep (Figure 4a; the somewhat nonmonotonic variations in G' in the high-frequency region are hypothesized to be a consequence of the high deformability of large LM droplets) and stress-ramp (Figure 4b) measurements. It should be recalled that the RSH products displayed k values comparable to those of the PS products at the corresponding LM loadings, which are also comparable to the reported values of various solid-state polymer/filler composites with high filler loadings above the percolation thresholds. Notably, this unprecedentedly high k-value improvement, while not causing the

https://doi.org/10.1021/acsomega.3c00487
ACS Omega 2023, 8, 17748−17757

vitrification of the resulted suspension, has not been achieved by any of the known solid fillers with high k_f values to the best of our knowledge. Thus, we suggest that the LM-in-oil emulsion produced via the RSH method has a high potential as a circulatable thermal transport fluid. Evidently, the LM droplets dispersed in this method were quite large and susceptible to gravitational sedimentation (Figure S4 in the Supporting Information). However, as the samples were continuously stirred magnetically for a prolonged time, simulating the case of continuous circulation, the back-scattering intensities of near-infrared (NIR, 808 nm) light irradiated to the sample vial measured at different storage times (up to a week) were very close (Figure 5), indicating that

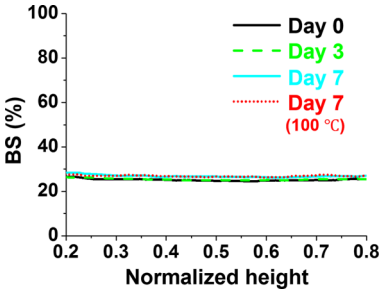

Figure 5. Intensity of the backscattered near-infrared light (BS in %; 880 nm; detected at 45°, where 0° is the irradiation direction) irradiated to the middle of the sample vial (normalized sample height ranging from 0.2 to 0.8; 0 and 1 are the sample bottom and top, respectively) containing the RSH-produced emulsion at an LM loading of 50 vol % for which continuous magnetic stirring was conducted at 100 rpm for a week.

there were minor variations in the droplet sizes and volume fractions in the samples under long-term convection. The thermal conductivity of the sample after stirring for a week was 0.784 W/m·K, which is very close to that of the initial sample, falling within the error margin. Furthermore, under stirring at an elevated temperature (100 °C, for which aqueous heat transfer fluids cannot be used), a week stability was confirmed (Figure 5). This suggests that the emulsion-type heat transfer fluids shown here would function properly if such fluids were continuously circulated by an external force.

The performance of the LM-in-oil emulsion produced via the RSH method as a heat transfer fluid was superior to that of the base fluid with no suspended LM droplets, as evaluated using custom-built test setups (Figure 6a,b). In the setup illustrated in Figure 6a, a borosilicate glass container (2.5 cm diameter, 6 cm height) filled with 10 mL of sample fluid with an initial temperature of ∼16 °C was placed on a heating plate at a constant temperature of 100 °C. While the sample container underwent natural convection owing to exposure to surrounding air (∼16 °C), the temperature rise over time at the middle of the sample fluid by heat transfer from the bottom was measured. The temperature rise of the LM-in-oil emulsion was remarkably faster than that of the base fluid, which is attributed to the higher thermal conductivity of the emulsion. Thus, the final temperature of the emulsion at 995 s was higher than that of the base fluid by approximately 5 °C, demonstrating the higher heating efficiency of the emulsion against the heat loss by natural convection. In the setup illustrated in Figure 6b, a smaller borosilicate glass container (1.4 cm diameter, 4.5 cm height) filled with 2 mL of heated water with an initial temperature of ∼75 °C was immersed in

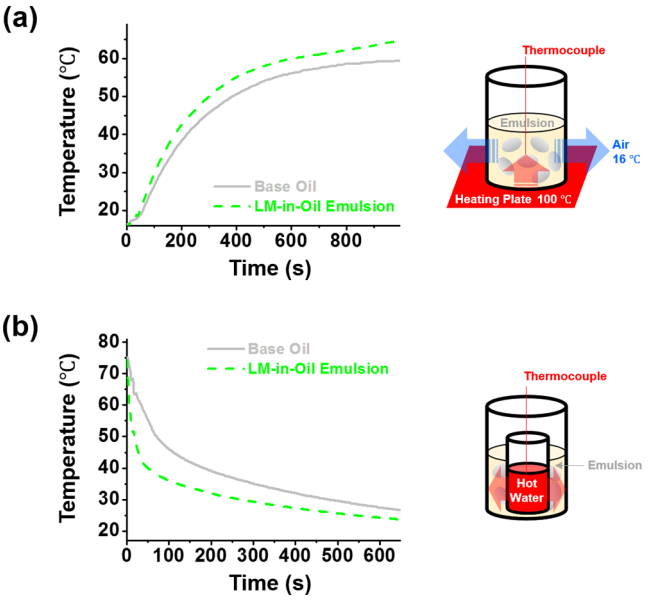

Figure 6. (a) Temperature rise in the base fluid and LM-in-oil emulsion in contact with a heating plate (100 °C) and exposed to surrounding air (∼16 °C). (b) Temperature drop of preliminarily heated water samples (∼75 °C) immersed in the base fluid and LM-in-oil emulsion (initially ∼16 °C). Schematics of the custom-built setups used for the two experiments are illustrated next to the respective temperature curves. The RSH-produced LM-in-oil emulsions used in (a) and (b) were at the maximum LM loading (50 vol %).

either the base fluid or emulsion (10 mL), which had an initial temperature of ∼16 °C, in the larger borosilicate glass container. The temperature drop over time at the middle of the inner water was then measured. In contrast to the case demonstrated in Figure 6a, oil-based fluids were used as coolants for the setup in Figure 6b. Evidently, the temperature drop of the inner water via the heat transfer to the outer oil was remarkably faster for the LM-in-oil emulsion than for the base fluid with no suspended LM droplets, which is attributed to the high thermal conductivity of the emulsion. While the test setups for conceptual demonstration shown herein are relatively simple, the superior heat transfer performances of the LM-in-oil emulsion over those of the normal oil are straightforward; therefore, the emulsion, particularly the high-fluidity emulsion from the RSH method, is expected to be useful as a heat transfer fluid in extended applications.

3. CONCLUSIONS

In this study, LM (EGaIn)-in-paraffin oil emulsions were produced at various LM loadings of up to 50 vol %, corresponding to an 89 wt % dispersed phase, using two different emulsification methods, i.e., PS and RSH. This high dispersed-phase loading has not been reported for previous heat transfer nanofluids published in the literature. Owing to the high volume fractions of dispersed high-k LM phase, substantial improvements in the overall emulsion k values were achieved, i.e., 0.98 ± 0.17 W/m·K (Δk (%) ∼ 409%) and 0.70 ± 0.16 W/m·K (Δk (%) ∼ 261%) for the PS- and RSH-produced emulsions at the maximum LM loading, respectively. These improvements in k values are comparable to the reported values for various polymer/filler composites with high conductive filler loadings, which are attributed to the enhanced

https://doi.org/10.1021/acsomega.3c00487
ACS Omega 2023, 8, 17748−17757

heat transport via high-k LM fillers with high loadings above the percolation threshold. Despite the very high dispersed-phase volume fractions, the produced emulsion, particularly that produced via the RHS method, demonstrated a remarkably high fluidity, exhibiting a relatively small low-shear-rate viscosity increase (i.e., within an order of magnitude) and $G'' > G'$ maintained up to the maximum investigated LM loading. The novel type of heat transfer emulsions shown in this study, with unprecedentedly high conductivity and fluidity combined, can be used in various applications where thermal energy transfer and utilization are required.

4. EXPERIMENTAL SECTION

4.1. Sample Preparation. Two different methods were used for the emulsification of LM in paraffin oils. In the probe-sonication (PS) method, the desired amounts of EGaIn (Changsha Santech Materials, China) were added to paraffin oil (SAMCHUN, Korea), which was preliminarily doped with 150 mM AOT (Sigma-Aldrich). The mixture was then probe-sonicated at an amplitude of 63 μm and a processing frequency of 20 kHz for 15 min using an HD 4200 probe sonicator (Bandelin, Germany) while being magnetically stirred at 700 rpm. In the rotor−stator homogenization (RSH) method, the corresponding amounts of EGaIn were added to the AOT-doped oils and shear-mixed using an HG-15D homogenizer (DAIHAN Scientific, Korea) at ∼11,000 rpm for 90 min.

4.2. Thermal Conductivity Measurements. The thermal conductivities of the emulsions (at 25 °C) were measured according to the ASTM E1530 standard using a DTC-300 (TA Instruments) guarded heat flow meter. In each measurement, sample emulsion was charged in a cylindrical cell (50.8 mm in diameter, 3.2 mm in height) with a side-guard furnace to prevent heat loss, to which a pneumatic load was applied with a thermal interface material. Heat flowed from the top to the bottom within the cell through the charged emulsion sample, and the temperature difference across the sample after reaching the equilibrium state was measured. The thermal conductivities of the emulsions were then calculated based on the measured temperature differences and sample thicknesses.

4.3. Rheological Measurements. A HAAKE MARS-40 rheometer (Thermo Fischer Scientific) with parallel plates with a diameter of 35 mm was used to measure the rheological properties of the LM-in-oil emulsions. Rotational viscosity measurements were performed in the shear rate range between 1 and 100 s^{-1}, using gap distances of 1 and 0.5 mm for the PS- and RSH-produced emulsions, respectively. The use of a smaller gap distance for the measurements of the RSH-produced emulsions was because of the relatively low sample viscosities. Oscillatory viscoelasticity measurements were also performed separately using frequency-sweep and stress-ramp modes. In the frequency-sweep mode, measurements were performed in the frequency range of 0.1−10 s^{-1} at a constant shear stress of 0.1 Pa. In the stress-ramp mode, measurements were performed in the stress range of 10^{-1}−10 Pa at a constant frequency of 0.1 s^{-1}. In both types of oscillatory measurements, the gap distance taken for the PS-produced emulsion was widened to 2.5 mm (from 1 mm) to avoid the destruction of the LM droplets packed in the high-viscosity sample; this produced reproducible results with relatively less noise.

4.4. Other Characterizations. A BX53M (Olympus, Japan) optical microscopy (OM) and a UHR FE-SEM (Hitachi, Japan) scanning electron microscopy (SEM) system were used to observe the morphologies of the produced LM droplets. JEM-2100F (JEOL, Japan) transmission electron microscopy (TEM) was used to observe the outermost surface of the LM droplets. An Aeries 600 (Malvern, U.K.) An X-ray diffractometer was used in the 2θ range of 5−80° to examine crystalline formation during emulsification. To analyze the oxidation states of the surfaces of the produced LM droplets, a Kα^+ (Thermo Fischer Scientific) X-ray photoelectron spectroscopy (XPS) apparatus with an Al Kα excitation source (1486.68 eV) was used. For depth profiling, Ar ion beam etching (0.5 keV, 1 mm × 1 mm raster size) was used. A Turbiscan Lab (Formulaction, France) was used to analyze the backscattering (45°) intensity of an 880 nm near-infrared (NIR) light irradiated to the sample that was magnetically stirred at 100 rpm for a week.

■ ASSOCIATED CONTENT

Supporting Information

The Supporting Information is available free of charge at https://pubs.acs.org/doi/10.1021/acsomega.3c00487.

SEM images of the PS- and RSH-produced LM droplets prepared at different LM loadings, the thermal conductivity of the "matrix" at various dopant (AOT) concentrations, the relative k values of the PS- and RSH-produced emulsions at various LM loadings, fitted to the Lewis−Nielsen model with a fixed maximum packing fraction of 1, and observation of the sedimentation behavior of RSH-produced LM droplets using a Turbiscan Lab instrument (PDF)

Demonstration of the fluidity of PS-produced emulsions (Movie S1) (MP4)

Demonstration of the fluidity of RSH-produced emulsions (Movie S2) (MP4)

■ AUTHOR INFORMATION

Corresponding Author

Joohyung Lee − *Department of Chemical Engineering, Myongji University, Yongin, Gyeonggi-do 17058, Korea;* orcid.org/0000-0001-6007-1052; Email: ljbro@mju.ac.kr

Authors

Suyeon Kim − *Department of Chemical Engineering, Myongji University, Yongin, Gyeonggi-do 17058, Korea*

Seongeun Kang − *Department of Chemical Engineering, Myongji University, Yongin, Gyeonggi-do 17058, Korea*

Complete contact information is available at: https://pubs.acs.org/10.1021/acsomega.3c00487

Notes

The authors declare no competing financial interest.

■ ACKNOWLEDGMENTS

This work was supported by the National Research Foundation of Korea (NRF) grant funded by the Korean government (MSIT) (2021R1F1A1048634). This research was supported by Nano·Material Technology Development Program through the National Research Foundation of Korea (NRF) funded by the Ministry of Science, ICT and Future Planning (2009-0082580).

REFERENCES

(1) Kulkarni, D. P.; Das, D. K.; Vajjha, R. S. Application of Nanofluids in Heating Buildings and Reducing Pollution. *Appl. Energy* **2009**, *86*, 2566−2573.

(2) Karakoyun, Y.; Acikgoz, O.; Kucukyildirim, B. O.; Yumurataci, Z.; Dalkilic, A. S. An Experimental Investigation on the Effect of Use of Nanofluids in Radiant Floor Heating Systems. *Energy Build.* **2021**, *252*, No. 111406.

(3) Zhao, N.; Li, S.; Yang, J. A Review on Nanofluids: Data-driven Modeling of Thermalphysical Properties and the Application in Automotive Radiator. *Renewable Sustainable Energy Rev.* **2016**, *66*, 596−616.

(4) Roe, C.; Feng, X.; White, G.; Li, R.; Wang, H.; Rui, X.; Li, C.; Zhang, F.; Null, V.; Parkes, M.; Patel, Y.; Wang, Y.; Wang, H.; Ouyang, M.; Offer, G.; Wu, B. Immersion Cooling for Lithium-ion Batteries − A Review. *J. Power Sources* **2022**, *525*, No. 231094.

(5) Hydratech Home Page, 2022. https://www.hydratech-usa.com/manufacturing. (accesses August 07, 2022).

(6) Joy, R. C.; Rajan, A. A.; Solomon, A. B.; Ramachandran, K.; Pillai, B. C. Experimental Investigation on the Critical Heat Flux of Cu-water, Al-water Nanofluids for Precise Cooling of Electronic Systems. *IOP Conf. Ser.: Mater. Sci. Eng.* **2019**, *561*, No. 012036.

(7) Birbarah, P.; Gebrael, T.; Foulkes, T.; Stillwell, A.; Moore, A.; Pilawa-Podgurski, R.; Miljkovic, N. Water Immersion Cooling of High Power Density Electronics. *Int. J. Heat Mass Transfer* **2020**, *147*, No. 118918.

(8) Tang, Z.; Qi, C.; Tian, Z.; Chen, L. Thermal Management of Electronic Components Based on New Wave Bio-inspired Structures and Nanofluids. *Int. Commun. Heat Mass Transfer* **2022**, *131*, No. 105840.

(9) Rubbi, F.; Das, L.; Habib, K.; Aslfattahi, N.; Saidur, R.; Alam, S. U. A Comprehensive Review on Advances of Oil-based Nanofluids for Concentrating Solar Thermal Collector Application. *J. Mol. Liq.* **2021**, *338*, No. 116771.

(10) Sharma, P.; Said, Z.; Kumar, A.; Nizetic, S.; Pandey, A.; Hoang, A. T.; Huang, Z.; Afzal, A.; Li, C.; Le, A. T.; Nguyen, X. P.; Tran, V. D. Recent Advances in Machine Learning Research for Nanofluid-Based Heat Transfer in Renewable Energy System. *Energy Fuels* **2022**, *36*, 6626−6658.

(11) Xuan, Y.; Li, Q. Heat Transfer Enhancement of Nanofluids. *Int. J. Heat Fluid Flow* **2000**, *21*, 58−64.

(12) Okonkwo, E. C.; Osho, I. W.; Kavaz, D.; Abid, M. Comparison of Experimental and Theoretical Methods of Obtaining the Thermal Properties of Alumina/Iron Mono and Hybrid Nanofluids. *J. Mol. Liq.* **2019**, *292*, No. 111377.

(13) Kumar, V.; Pandya, N.; Pandya, B.; Joshi, A. Synthesis of Metal-based Nanofluids and Their Thermo-hydraulic Performance In Compact Heat Exchanger with Multi-louvered Fins Working Under Laminar Conditions. *J. Therm. Anal. Calorim.* **2019**, *135*, 2221−2235.

(14) Sen, S.; Govindarajan, V.; Pelliccione, C. J.; Wang, J.; Miller, D. J.; Timofeeva, E. V. Surface Modification Approach to TiO2 Nanofluids with High Particle Concentration, Low Viscosity, and Electrochemical Activity. *ACS Appl. Mater. Interfaces* **2015**, *7*, 20538−20547.

(15) Saeed, M.; Kim, M.-H. Heat Transfer Enhancement Using Nanofluids (Al2O3-H2O) in Mini-channel Heatsinks. *Int. Commun. Heat Mass Transfer* **2018**, *120*, 671−682.

(16) Bao, Z.; Bing, N.; Zhu, X.; Xie, H.; Yu, W. Ti3C2Tx MXene Contained Nanofluids with High Thermal Conductivity, Super Colloidal Stability and Low Viscosity. *Chem. Eng. J.* **2021**, *406*, No. 126390.

(17) Chen, W.; Zhou, C.; Li, X. Application of Large-scale Prepared MWCNTs Nanofluids in Solar Energy System as Volumetric Solar Absorber. *Sol. Energy Mater. Sol. Cells* **2019**, *200*, No. 109931.

(18) Brzóska, K.; Jóźwiak, B.; Golba, A.; Dzida, M.; Boncel, S. Thermophysical Properties of Nanofluids Composed of Ethylene Glycol and Long Multi-Walled Carbon Nanotubes. *Fluids* **2020**, *5*, No. 241.

(19) Swapna, M. N. S.; Raj, V.; Cabrera, H.; Sankararaman, S. I. Thermal Lensing of Multi-walled Carbon Nanotube Solutions as Heat Transfer Nanofluids. *ACS Appl. Nano Mater.* **2021**, *4*, 3416−3425.

(20) Choi, S. U. S.; Eastman, J. A. Enhancing Thermal Conductivity of Fluids with Nanoparticles, Argonne National Laboratory Report ANL/MSD/CP-84938, 1995. https://www.osti.gov/servlets/purl/196525. (accesses August 07, 2022).

(21) Das, S. K.; Choi, S. U. S.; Patel, H. E. Heat Transfer in Nanofluids − A Review. *Heat Transfer Eng.* **2006**, *27*, 3−19.

(22) Saidur, R.; Leong, K. Y.; Mohammed, H. A. A Review on Applications and Challenges of Nanofluids. *Renewable Sustainable Energy Rev.* **2011**, *15*, 1646−1668.

(23) Okonkwo, E. C.; Wole-Osho, I.; Almanassra, I. W.; Abdullatif, Y. M.; Al-Ansari, T. An updated review of nanofluids in various heat transfer devices. *J. Therm. Anal. Calorim.* **2021**, *145*, 2817−2872.

(24) Menni, Y.; Chamkha, A. J.; Lorenzini, G.; Kaid, N.; Ameur, H.; Bensafi, M. Advances of Nanofluids in Solar Collectors−a Review of Numerical Studies. *Math. Modell. Eng. Probl.* **2019**, *6*, 415−427.

(25) Wahab, A.; Hassan, A.; Qasim, M. A.; Ali, H. M.; Babar, H.; Sajid, M. U. Solar Energy Systems−Potential of Nanofluids. *J. Mol. Liq.* **2019**, *289*, No. 111049.

(26) Krishna, V. M.; Kumar, M. S. Numerical Analysis of Forced Convective Heat Transfer of Nanofluids in Microchannel for Cooling Electronic Equipment. *Mater. Today: Proc.* **2019**, *17*, 295−302.

(27) Ibrahim, H.; Sazali, N.; Shah, A. S. M.; Karim, M. S. A.; Aziz, F.; Salleh, W. N. W. A Review on Factors Affecting Heat Transfer Efficiency of Nanofluids for Application in Plate Heat Exchanger. *J. Adv. Res. Fluid Mech. Therm. Sci.* **2019**, *60*, 144−154.

(28) Sajid, M. U.; Ali, H. M. Recent Advances in Application of Nanofluids in Heat Transfer Devices: A Critical Review. *Renewable Sustainable Energy Rev.* **2019**, *103*, 556−592.

(29) Qiu, L.; Zhu, N.; Feng, Y.; Michaelides, E. E.; Zyta, G.; Jing, D.; Zhang, X.; Norris, P. M.; Markides, C. N.; Mahian, O. A Review of Recent Advances in Thermophysical Properties at the Nanoscale: From Solid State to Colloids. *Phys. Rep.* **2020**, *843*, 1−81.

(30) Choi, S. U. S.; Zhang, Z. G.; Yu, W.; et al. Anomalous Thermal Conductivity Enhancement in Nanotube Suspensions. *Appl. Phys. Lett.* **2001**, *79*, 2252−2254.

(31) Nielsen, L. E. Thermal Conductivity of Particulate-Filled Polymers. *J. Appl. Polym. Sci.* **1973**, *17*, 3819−3820.

(32) Nielsen, L. E. The Thermal and Electrical Conductivity of Two-Phase Systems. *Ind. Eng. Chem. Fundam.* **1974**, *13*, 17−20.

(33) Agari, Y.; Uno, T. Estimation on Thermal Conductivities of Filled Polymers. *J. Appl. Polym. Sci.* **1986**, *32*, 5705−5712.

(34) Pietrak, K.; Winiewski, T. S. A Review of Models for Effective Thermal Conductivity of Composite Materials. *J. Power Technol.* **2015**, *95*, 14−24.

(35) Burger, N.; Laachachi, A.; Ferriol, M.; Lutz, M.; Toniazzo, V.; Ruch, D. Review of Thermal Conductivity in Composites: Mechanisms, Parameters and Theory. *Prog. Polym. Sci.* **2016**, *61*, 1−28.

(36) Xu, Y.; Chung, D. D. L.; Mroz, C. Thermally Conducting Aluminum Nitride Polymer-Matrix Composites. *Composites, Part A* **2001**, *32*, 1749−1757.

(37) Kargar, F.; Barani, Z.; Salgado, R.; Debnath, B.; Lewis, J. S.; Aytan, E.; Lake, R. K.; Balandin, A. A. Thermal Percolation Threshold and Thermal Properties of Composites with High Loading of Graphene and Boron Nitride Fillers. *ACS Appl. Mater. Interfaces* **2018**, *10*, 37555−37565.

(38) Shin, H.; Ahn, S.; Kim, D. H.; Lim, J. K.; Kim, C. B.; Goh, M. Recyclable Thermoplastic Hexagonal Boron Nitride Composites with High Thermal Conductivity. *Composites, Part B* **2019**, *163*, 723−729.

(39) Xiao, C.; Chen, L.; Tang, Y.; Zhang, X.; Zheng, K.; Tian, X. Three Dimensional Porous Alumina Network for Polymer Composites with Enhanced Thermal Conductivity. *Composites, Part A* **2019**, *124*, No. 105511.

(40) Zhang, G.; Xia, Y.; Wang, H.; Tao, Y.; Tao, G.; Tu, S.; Wu, H. A Percolation Model of Thermal Conductivity for Filled Polymer Composites. *J. Compos. Mater.* **2010**, *44*, 963−970.

https://doi.org/10.1021/acsomega.3c00487
ACS Omega 2023, 8, 17748−17757

(41) Tong, X. C. *Advanced Materials for Thermal Management of Electronic Packaging*; Springer: New York, 2011.
(42) Bartlett, M. D.; Kazem, N.; Powell-Palm, M. J.; Huang, X.; Sun, W.; Malen, J. A.; Majidi, C. High Thermal Conductivity in Soft Elastomers with Elongated Liquid Metal Inclusions. *Proc. Natl. Acad. Sci. U.S.A.* **2017**, *114*, 2143−2148.
(43) Jia, L.-C.; Jin, Y.-F.; Ren, J.-W.; Zhao, L.-H.; Yan, D.-X.; Li, Z.-M. Highly Thermally Conductive Liquid Metal-based Composites with Superior Thermostability for Thermal Management. *J. Mater. Chem. C* **2021**, *9*, 2904−2911.
(44) Krings, E. J.; Zhang, H.; Sarin, S.; Shield, J. E.; Ryu, S.; Markvicka, E. J. Lightweight, Thermally Conductive Liquid Metal Elastomer Composite with Independently Controllable Thermal Conductivity and Density. *Small* **2021**, *17*, No. 2104762.
(45) Bark, H.; Tan, M. W. M.; Thangavel, G.; Lee, P. S. Deformable High Loading Liquid Metal Nanoparticles Composites for Thermal Energy Management. *Adv. Energy Mater.* **2021**, *11*, No. 2101387.
(46) Moon, S.; Kim, H.; Lee, K.; Park, J.; Kim, Y.; Choi, S. Q. 3D Printable Concentrated Liquid Metal Composite with High Thermal Conductivity. *iScience* **2021**, *24*, No. 103183.
(47) Chen, S.; Xing, W.; Wang, H.; Cheng, W.; Lei, Z.; Zheng, F.; Tao, P.; Shang, W.; Fu, B.; Song, C.; Dickey, M. D.; Deng, T. A Bottom-up Approach to Generate Isotropic Liquid Metal Network in Polymer-enabled 3D Thermal Management. *Chem. Eng. J.* **2022**, *439*, No. 135674.
(48) Daeneke, T.; Khoshmanesh, K.; Mahmood, N.; de Castro, I. A.; Esrafilzadeh, D.; Barrow, S. J.; Dickey, M. D.; Kalantar-zadeh, K. Liquid Metals: Fundamentals and Applicationsin Chemistry. *Chem. Soc. Rev.* **2018**, *47*, 4073−4111.
(49) Yu, S.; Kaviany, M. Electrical, Thermal, and Species Transport Properties of Liquid Eutetctic Ga-In and Ga-In-Sn from First Principles. *J. Chem. Phys.* **2014**, *140*, No. 064303.
(50) Li, Z.; Zhang, H.; Wang, D.; Gao, C.; Sun, M.; Wu, Z.; He, Q. Reconfigurable Assembly of Active Liquid Metal Colloidal Cluster. *Angew. Chem., Int. Ed.* **2020**, *59*, 19884−19888.
(51) Kim, J.; Jeong, J.; Hyum, Y.; Chung, S. K.; Lee, J. Electrostatic Stabilization of Nano Liquid Metals in Doped Nonpolar Liquids. *Small* **2021**, *17*, No. 2104143.
(52) Kim, J.; Lee, J. Liquid-Suspended and Liquid-Bridged Liquid Metal Microdroplets. *Small* **2022**, *18*, No. 2108069.
(53) Lee, J.; Yezer, B. A.; Prieve, D. C.; Behrens, S. H. Janus Particles in a Nonpolar Solvent, 32. *Langmuir* **2016**, 3095−3099.
(54) Park, H.; Lim, S.; Yang, J.; Kwak, C.; Kim, J.; Kim, J.; Choi, S. S.; Kim, C. B.; Lee, J. A Systematic Investigation on the Properties of Silica Nanoparticles "Multipoint"-Grafted with Poly(2-Acrylamido-2-Methylpropanesulfonate-co-Acrylic Acid) in Extreme Salinity Brines and Brine-Oil Interfaces. *Langmuir* **2020**, *36*, 3174−3183.
(55) Son, Y.; Lim, M.; Kim, J. Investigation of Acoustic Cavitation Energy in a Large-scale Sonoreactor. *Ultrason. Sonochem.* **2009**, *16*, 552−556.
(56) Yusof, N. S. M.; Babgi, B.; Alghamdi, Y.; Aksu, M.; Madhavan, J.; Ashokkumar, M. Physical and Chemical Effects of Acoustic Cavitation in Selected Ultrasonic Cleaning Applications. *Ultrason. Sonochem.* **2016**, *29*, 568−576.
(57) Homogenizers.net Home Page, 2022. https://homogenizers.net/. (accesses August 07, 2022).
(58) Hutter, T.; Bauer, W.-A. C.; Elliott, S. R.; Huck, W. T. S. Formation of Spherical and Non-Spherical Eutectic Gallium-Indium Liquid-Metal Microdroplets in Microfluidic Cannels at Room Temperature. *Adv. Funct. Mater.* **2012**, *22*, 2624−2631.
(59) Lin, Y.; Liu, Y.; Genzer, J.; Dickey, M. D. Shape-transformable Liquid Metal Nanoparticles in Aqueous Solution. *Chem. Sci.* **2017**, *8*, 3832−3837.
(60) Yan, J.; Zhang, X.; Liu, Y.; Ye, Y.; Yu, J.; Chen, Q.; Wang, J.; Zhang, Y.; Hu, Q.; Kang, Y.; Yang, M.; Gu, Z. Shape-controlled Synthesis of Liquid Metal Nanodroplets for Photothermal Therapy. *Nano Res.* **2019**, *12*, 1313−1320.
(61) Zhang, M.; Liu, L.; Zhang, C.; Chang, H.; Zhang, P.; Rao, W. Self-Foaming as a Universal Route for Fabricating Liquid Metal Foams and Hollow Particles. *Adv. Mater. Interfaces* **2021**, *8*, No. 2100432.
(62) Tevis, I. D.; Newcomb, L. B.; Thuo, M. Synthesis of Liquid Core-Shell Particles and Solid Patch Multicomponent Particles by Shearing Liquids Into Complex Particles (SLICE). *Langmuir* **2014**, *30*, 14308−14313.
(63) Lee, J.; Jung, S.; Kim, W. Dependence of the Effective Surface Tension of Liquid Phae Eutectic Gallium Indium on Wrinkles of the Surface Oxide. *Extreme Mech. Lett.* **2021**, *48*, No. 101386.
(64) Shah, N. U. H.; Kong, W.; Casey, N.; Kanetkar, S.; Wang, R. Y.; Rykaczewski, K. Gallium Oxide-Stabilized Oil in Liquid Metal Emulsions. *Soft Matter* **2021**, *17*, 8269−8275.
(65) Compton, B. G.; Lewis, J. A. 3D-Printing of Lightweight Cellular Composites. *Adv. Mater.* **2014**, *26*, 5930−5935.
(66) Kwak, C.; Ryu, S. Y.; Park, H.; Lim, S.; Yang, J.; Kim, J.; Kim, J. H.; Lee, J. A Pickering Emulsion Stabilized by Chlorella Microalgae as an Eco-friendly Extrusion-based 3D Printing Ink Processable Under Ambient Conditions. *J. Colloid Interface Sci.* **2021**, *582*, 81−89.
(67) Larson, R. G. *The Structure and Rheology of Complex Fluids*; Oxford University Press: New York, 1999.
(68) Alger, M. *Polymer Science Dictionary*, 3rd ed.; Springer: Dordrecht, 2017.
(69) Pabst, W.; Gregorova, E.; Bertold, C. Particle-Shape and Suspension Rheology of Sort-fiber Systems. *J. Eur. Ceram. Soc.* **2006**, *26*, 149−160.
(70) Mueller, S.; Llewellin, E. W.; Mader, H. M. The Rheology of Suspensions of Solid Particles. *Proc. R. Soc. A* **2010**, *466*, 1201−1228.
(71) Rintoul, M. D.; Torquato, S. Computer Simulations of Dense Hard-sphere Systems. *J. Chem. Phys.* **1996**, *105*, 9258−9265.
(72) Chang, C.; Powell, R. L. Effect of Particle Size Distributions on the Rheology of Concentrated Bimodal Suspensions. *J. Rheol.* **1994**, *38*, 85−98.
(73) Luckham, P. F.; Ukeje, M. A. Effect of Particle Size Distribution on the Rheology of Dispersed Systems. *J. Colloid Interface Sci.* **1999**, *220*, 347−356.
(74) Saiki, Y.; Prestidge, C. A.; Horn, R. G. Effects of Droplet Deformability on Emulsion Rheology. *Colloids Surf., A* **2007**, *299*, 65−72.
(75) Krieger, I. M.; Dougherty, T. J. A Mechanism for Non-Newtonian Flow in Suspensions of Rigid Spheres. *Trans. Soc. Rheol.* **1959**, *3*, 137−152.
(76) Zhang, Z. M. *Nano/Microscale Heat Transfer*; McGraw-Hill: New York, 2007.
(77) Mason, T. G.; Weitz, D. A. Linear Viscoelasticity of Colloidal Hard Sphere Suspensions near the Glass Transition. *Phys. Rev. Lett.* **1995**, *75*, 2770−2773.
(78) Yang, J.; Park, H.; Kim, J.; Mok, J.; Kim, T.; Shin, E.; Kwak, C.; Lim, S.; Kim, C. B.; Park, J.-S.; Na, H. B.; Choi, D.; Lee, J. Yield Stress Enhancement of a Ternary Colloidal Suspension via the Addition of Minute Amounts of Sodium Alginate to the Interparticle Capillary Bridges. *Langmuir* **2020**, *36*, 9424−9435.

https://doi.org/10.1021/acsomega.3c00487
ACS Omega 2023, 8, 17748−17757